JOURNAL OF GEOPHYSICAL RESEARCH, VOL. 106, NO. D14, PAGES 14,919–14,934, JULY 27, 2001

Saharan dust in Brazil and Suriname during the Large-Scale Biosphere-Atmosphere Experiment in Amazonia (LBA) – Cooperative LBA Regional Experiment (CLAIRE) in March 1998

P. Formenti,[1,2] M. O. Andreae,[1] L. Lange,[1,2] G. Roberts,[1] J. Cafmeyer,[3] I. Rajta,[3] W. Maenhaut,[3] B. N. Holben,[4] P. Artaxo,[5] and J. Lelieveld[2]

Abstract. Advection of Saharan dust was observed via chemical and optical measurements during March 1998 in Brazil and Suriname during the Large-Scale Biosphere-Atmosphere Experiment in Amazonia (LBA)-Cooperative LBA Airborne Regional Experiment (CLAIRE)-98 experiment. In Brazil the dust outbreak produced an increase of a factor of 3 in the daily mean mass concentration (up to 26 ± 7 μg m^{-3}) of particles smaller than 10 μm equivalent aerodynamic diameter (EAD), and in the daily mean aerosol particle scattering coefficient σ_s (up to 26 ± 8 Mm^{-1} STP, ambient humidity). Background levels of aerosol scattering (ambient) were $\sigma_s \sim 10$ Mm^{-1}. The effect of dust advection was evident for all major crustal elements (Al, Si, Ca, Ti, Mn, and Fe), as well as the sea-salt elements (Na, Cl, and S), as the dust layer was transported at low altitude (below 800 hPa). Coarse P and organic carbon (OC) concentrations were not influenced by the occurrence of dust, and were mainly emitted by the rain forest. The dry scattering mass efficiency of dust (particles smaller than 10 μm EAD) was estimated to be between 0.65 (± 0.06) and 0.89 (± 0.08) m^2 g^{-1}. Airborne profiles of aerosol scattering showed two distinct types of vertical structure in the dust layer over Suriname, either vertically uniform (15, 26 March), or plume-like (25 March). Dust layers extended generally up to 700 hPa, while scattering layers occasionally encountered at higher altitudes resulted from smoke emitted by biomass burning in Venezuela and Colombia. Observations in South America were supported by measurements in Israel and Tenerife (Canary Islands), where the dust outbreaks were also detected.

1. Introduction

The large-scale movement of dust aerosol plumes originating over northern Africa has been extensively studied by in situ and remote sensing observations [*Prospero and Carlson*, 1972; *Husar et al.*, 1997; *Prospero*, 1999], as well as by model calculations [*Tegen and Lacis*, 1996]. Windstorms over the Sahara/Sahel region can mobilize up to 700 Tg (1 Tg = 10^{12} g) of mineral dust per year [*Chiapello et al*, 1997, and references therein], injecting nutrients and crustal material to forests, and terrestrial and deep-sea sediments [*Swap et al*, 1992; *Chiapello et al*, 1997] Dust particles scatter solar light in the visible spectral region and absorb thermal terrestrial radiation in the infrared [*Andreae*, 1996, *Tegen and Lacis*, 1996]. This twofold radiative role has complex climatic implications that are far from being completely understood [*Andreae*, 1996]. Severe deterioration of visibility due to sudden increases of windblown dust concentrations may also cause hazards to air traffic [*Ganor*, 1994]. A major route of transport of wind-blown dust from the Sahara is across the North Atlantic Ocean westward toward the American continent [*Prospero and Carlson*, 1972; *Prospero*, 1999]. Owing to the north-south oscillation of the Intertropical Convergence Zone (ITCZ), in winter the dust plume travels south of 20°N toward the Amazon basin [*Prospero et al.*, 1981; *Swap et al.*, 1992], while in summer it travels prevalently north of 20°N toward Central and North America [*Perry et al*, 1997; *Prospero*, 1999]. During winter-spring, eastward transport is also strong toward Europe and the Middle East [*Ganor*, 1994; *Moulin et al*, 1998].

During March 1998, Total Ozone Mapping Spectrometer (TOMS), Meteosat and Advanced Very High Resolution Radiometer (AVHRR) satellite images showed that mobilization of mineral dust from the Sahara was intense. This was especially true during 14–16 March and 23–27 March, when major dust plumes were detected moving toward South America and the Middle East. During 14–16 March, a "dust alert", that is, a notification of major increase of dust concentration in the atmosphere, was given for the eastern Mediterranean basin on the basis of the Mediterranean Dust Experiment (MEDUSE) model predictions (http://ff.halo.hi.is/meduse/). The predictions for the aerosol column load over Israel were of the order of 4500 mg m^{-2}.

In this paper we focus on the ground-based and airborne observations for the dust episode of 23–27 March conducted in Brazil and Suriname as part of the Large-Scale Biosphere-Atmosphere Experiment in Amazonia (LBA)-Cooperative LBA Airborne Regional Experiment (CLAIRE)-98, hereafter referred to simply as CLAIRE intensive experiment. When appropriate, results from additional ground-based sites (Israel and Tenerife) are used.

[1] Biogeochemistry Department, Max Planck Institute for Chemistry, Mainz, Germany.
[2] Institute for Marine and Atmospheric Research (IMAU), University of Utrecht, Utrecht, Netherlands.
[3] Institute for Nuclear Sciences, University of Gent, Gent, Belgium.
[4] Biospheric Sciences Branch, NASA Goddard Space Flight Center, Greenbelt, Maryland.
[5] Instituto de Física, Universidade de São Paulo, São Paulo, Brazil.

Paper number 2000JD900827
0148-0227/01/2000JD900827$09 00

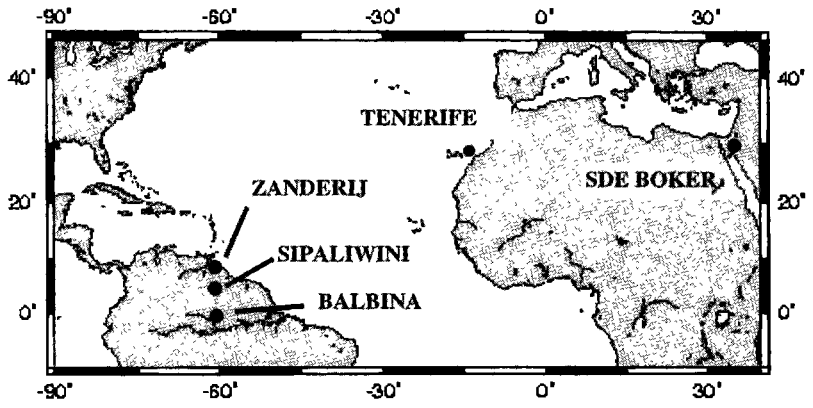

Figure 1. Location of the sampling sites during March 1998.

2. Sampling Sites

The locations of the five sites at which the dust events were observed are indicated in Figure 1. These are as follows:

1. Balbina (1°55'S, 59°24'W; 174 m above sea level (asl)), Brazil, is located approximately 100 km north of Manaus and faces more than 1000 km of pristine forest in the prevailing wind direction. Here ground-based observations of physical, optical, and chemical properties of the atmospheric aerosol were made from 23 March to 14 April 1998. We measured scattering (σ_s) and absorption (σ_a) coefficients (both at ambient conditions), size-separated mass (fine particle mass (FPM) and coarse particle mass (CPM)), organic carbon (OC), elemental and black carbon (EC, BC) and elemental concentrations, and total suspended particulate (TSP) mass concentrations.

2. Two sites are located in Suriname: Zanderij airport (5°47'N, 55°12'W; 10 m asl) and Sipaliwini (2°12'N, 56°06'W; 330 m asl). The Zanderij airport site is located near the coast and it is part of the Aerosol Robotic Network (AERONET) Sun/sky photometer network managed by NASA Goddard Space Flight Center [*Holben et al*, 1998]. The 10 CLAIRE measurement flights were conducted from Zanderij offshore and over Suriname (12–28 March). Zanderij also hosted ground-based measurements of spectral aerosol optical depth, τ_a, and sampling of some size-segregated aerosol samples. These were collected also at Sipaliwini, located 500 km inland, within the rain forest.

3. Sde Boker (30°51'N, 34°47'E; 470 m asl), Israel, hosts continuous ground-based measurements of the aerosol particle scattering coefficient, σ_s, and of fine and coarse particle mass, BC, and elemental concentrations.

4. Mount Teide (28°27'N, 16°63'W; 3570 m asl), Tenerife, Spain, was a site for ground-based measurements of spectral τ_a.

An AERONET site is also operating at the Cape Verde Islands, 500 km west of the African coast of Senegal, but measurements were not available during March 1998 (B. Chatenet, personal communication, 1999).

3. Methodology

3.1. Optical Measurements

3.1.1. Measurements of aerosol scattering coefficient (σ_s). Airborne measurements over Suriname were performed with a Cessna Citation II twin-jet aircraft. On board the aircraft, the aerosol particle scattering coefficient σ_s was measured at 545 nm by a single-wavelength nephelometer (M903, Radiance Research, Seattle, Washington). At a flow rate of 2–3 L min^{-1} the backward-pointing 1/4 inch inlet on the aircraft provided an upper cutoff at approximately 1 μm diameter, so that only the fine fraction of the dust layer was sampled. Because of the very high temperatures in the aircraft, the relative humidity inside the nephelometer chamber never exceeded 50%, and σ_s was measured under dry conditions. Two identical devices were operated on the ground in Balbina and in Sde Boker. There, σ_s was measured under ambient conditions. The measurements of the scattering coefficient σ_s are reported in Mm^{-1}, that is, 10^{-6} m^{-1}. When used, standard pressure and temperature (STP) conditions referred to $p = 1013.25$ hPa, $T = 293$ K. No corrections for near-forward truncation and Lambertian nonidealities were made to the scattering data used in this study. Correction factors for total scattering depend on the particle size, and may be expressed as a linear function of the Ångström exponent for scattering [*Anderson and Ogren*, 1998]. This information was not available at our sampling sites, if not (section 3.1.2) integrated over the whole atmospheric column. For the Radiance Research nephelometer, σ_s for particles smaller than 10 μm diameter is underestimated by about 32% (H. Maring, personal communication, 2000). The uncertainty introduced by this correction is at least 25%.

3.1.2. Measurements of aerosol optical depths (τ_a). At Zanderij, ground-based spectral aerosol optical depth (τ_a) and sky brightness were measured at 440, 500, 670, 870 and 1020 nm by a sun/sky photometer (CE318, CIMEL Electronique, Paris, France). An error of ± 0.01 is associated with the measurement [Holben et al., 1998]. The sky brightness spectra are used to retrieve column aerosol size distribution [*Dubovik et al*, 2000].

At Mount Teide, τ_a at 415, 501, 615, 675, and 868 nm was measured with a multifilter rotating shadow-band radiometer (MFRSR7, Yankee Environmental System, Inc, Turner Falls, Massachusetts). Mathematical retrieval of the column aerosol size distribution from the spectral τ_a was done using the algorithm of *King et al* [1978].

3.2. Chemical Measurements

Aerosol samples for chemical analysis were taken at Balbina, Zanderij, Sipaliwini, and Sde Boker. The size-segregated concentrations for elements from Na to Th in the fine (particle equivalent aerodynamic diameter (EAD) < 2 μm) and coarse (2 μm < EAD < 10 μm) fractions were obtained by SFU (stacked

filter unit) sampling on Nuclepore polycarbonate filters coupled with PIXE (particle induced X-ray emission) and INAA (instrumental neutron activation analysis) analysis [*Maenhaut and Zoller*, 1977; *Maenhaut and Raemdonck*, 1984]. The collection time per sample varied between 1 and 2 days. BC concentrations were measured via a light reflection technique [*Andreae*, 1983; *Andreae et al.*, 1984]. As this technique may be influenced by light-absorbing species other than black carbon, and because the cross section of black carbon varies with aerosol aging and mixing state, the BC measured by this method is referred to as black carbon equivalent (BCE). FPM and CPM were determined by weighing at 20°C and 50% relative humidity. The total suspended particulate (TSP) mass (by weighing) and organic carbon (OC) and elemental carbon (EC) concentrations (via a thermal-optical transmission technique [*Birch and Cary*, 1996]) were also obtained. The OC and EC data were derived from aerosol collections with Whatman QM-A quartz fiber filters.

Highly size-segregated aerosol samples (12 fractions in the size range 0.045–15 μm EAD) were collected using a small-deposit-area low-pressure impactor (SDI) [*Maenhaut et al.*, 1996a]. The SDI was operated at a flow rate of 11 L min^{-1} At this flow rate, cut points were 8 5, 4.1, 2 7, 1 7, 1.1, 0.77, 0.59, 0.34, 0.23, 0 15, 0.086 and 0 045 μm. These cut points are to be interpreted as the lower limits for the size range collected by the stage. Samples were analyzed using PIXE only.

3.3. Back Trajectory Calculations

Three-dimensional air mass trajectories were calculated with the KNMI [*Scheele et al*, 1996] and the National Oceanic and Atmospheric Administration (NOAA) HYbrid Single-Particle Lagrangian Integrated Trajectory Model (HYSPLIT4) [*Draxler and Hess*, 1997] models. The KNMI model calculated 10-day back trajectories at five end pressure levels (975, 850, 700, 500, and 300 hPa) using 3-D wind fields from European Centre for Medium-Range Weather Forecasts (ECMWF) analyses. The HYSPLIT4 model was used to calculate 5- and 10-day back and forward trajectories at user-defined pressure levels between 960 and 200 hPa. The meteorological data set used is the FNL ("final") 3-D data set obtained from the National Weather Service's National Centers for Environmental Prediction (NCEP) analysis.

4. General Meteorology During March 1998

In March the ITCZ is located at approximately 1°N Suriname therefore lies almost entirely in the meteorological Northern Hemisphere, while Brazil, including Balbina, is located in the Southern Hemisphere. During the January–April period the airflow over the lowest 5–6 km of the atmosphere in most of the study area is dominated by a NE trade wind flow, which transports humid oceanic air masses over the forests of Suriname and the Guyanas and from there on into the Amazon basin.

March 1998 was characterized by anomalously dry weather conditions, probably due to the effects of El Niño (W. Peters, unpublished report, 1998) This resulted in enhanced biomass burning in parts of Brazil, Suriname and neighboring countries. Large fires were observed in Roraima State (northwestern Brazil), at the border with Venezuela. These are evident as "hot spots" in the aerosol absorption satellite maps retrieved by TOMS [*Herman et al*, 1997]. Examples are shown in Figure 2 for 17 and 25 March; the aerosol plumes traveling from Africa are also evident. Local biomass burning activity occurred in coastal Suriname, although on a much smaller scale. AVHRR images of Central America (http://hazard1.wwb.noaa.gov/) showed forest fires also in Panama, Mexico, and Costa Rica.

5. Observations in Suriname

5.1. Optical Properties of the Dust Layers

The airborne nephelometer vertical soundings over Suriname on 25 and 26 March (Figures 3a and 3b) showed a complex vertical structure with several biomass burning and dust plumes. The flight patterns on these two days were almost identical, and were based on a north–south transect at varying altitudes (Figure 4). The sharp peak observed on 25 March at 400 hPa (σ_s up to 31 Mm^{-1} STP) coincided with a peak in CO concentrations and was associated with air masses that had traveled over Central America and Venezuela; therefore it probably represented a biomass burning plume. Because this air mass had remained in the Northern Hemisphere and had not crossed the ITCZ, it still carried a significant amount of aerosols in the accumulation mode (the more optically active size region) This implies a different transport mechanism from the lofting of biomass burning plumes by deep convection through the ITCZ, which was observed on 26 March at 200 hPa where significant depletion of accumulation mode particles had occurred [*Andreae et al*, 2001]. There was no evidence of such aerosol-depleted plumes in the nephelometer soundings from the flights discussed here (Figure 3b). A slight enhancement of σ_s, likely due to biomass burning over Venezuela, was, however, observed on this same day at 650 hPa

On 25 March (Figure 3a), layers of African dust were transported within the easterly trade winds at altitudes below 500 hPa. A double-layer structure around 700 and 600 hPa was occasionally observed. Dilution and subsidence of the dust layers occurred as the air moved inland over Suriname. The mean σ_s on the dust layer sampled during the northernmost profile was 34 ± 21 Mm^{-1} (average pressure level 700 hPa), while on the southernmost profile σ_s was 15 ± 6 Mm^{-1} (average pressure level 800 hPa). The overall shape of the layer was preserved. The southernmost position reached during the inland profiles was approximately 2°N, still north of the ITCZ.

On 26 March, the synoptic circulation pattern shifted toward an anticyclonic regime. Air masses below 700 hPa originated in the Gulf of Mexico, but resided offshore Suriname (where TOMS images showed a heavy load of absorbing aerosols) for as long as 3 days, during which they mixed with the Saharan plume arriving from the east Again (Figure 3b) the two northernmost (coastal) profiles (average σ_s below 700 hPa between 8 ± 3 and 15 ± 12 Mm^{-1} STP) were enriched with respect to the four inland profiles (mean σ_s between 1.5 and 1.9 Mm^{-1} STP). However, the vertical structure was very different from the previous day. Most inland profiles were identical, showing that the aerosol load over the rain forest was uniform, both horizontally and vertically (σ_s almost constant up to 700 hPa). The magnitude of the scattering was significantly lower than on the previous day, when values never were below 10 Mm^{-1}. The coastal profiles did not show any structural evidence of a dust plume. This evolution is evident also in the time series of spectral τ_a measured at the airport site (Figure 5). Despite the scarcity of data on 23–24 March, the progressive decrease of τ_a (from 0.7 on 23 March to 0.15 on 26 March at 500 nm) together with a progressive increase of the Ångström exponent (from 0.1–0.3 on 23–24 and part of 25 March

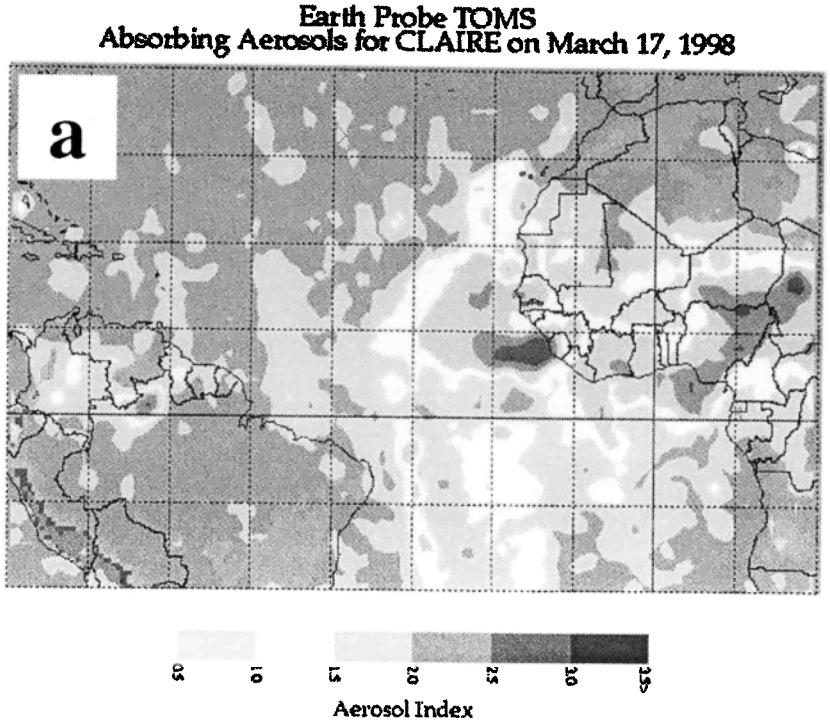

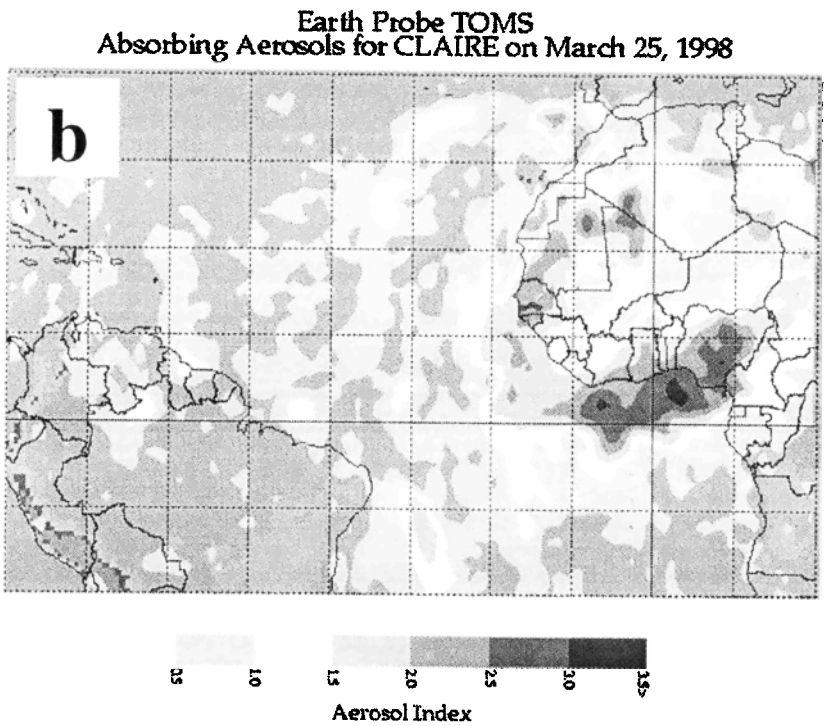

Figure 2. Total Ozone Mapping Spectrometer (TOMS) satellite images of absorbing aerosols for (a) 17 March and (b) 25 March, 1998 showing the intense forest fires over the Roraima state (Brazil) as well as the transport of Saharan mineral dust across the Atlantic Ocean.

to 0.3–0 7 on late 25 and on 26 March) indicates a transition from dust-only to mixed conditions.

5.1.1. Comparison of ground-based and airborne measurements. Ground-based τ_a were compared with the scattering optical depth τ_s obtained from the vertical integration of the σ_s profile measured with the aircraft. Ongoing balloon soundings from the Research on Atmospheric Dynamics and Chemistry in Suriname (RADCHiS) program shows that during March the relative humidity RH near the surface in Suriname continuously exceeds the 70% level and is often as high as 80-90%. The RH drops quickly with height, and only occasionally exceeds 50% above 2 km altitude (W. Peters, personal

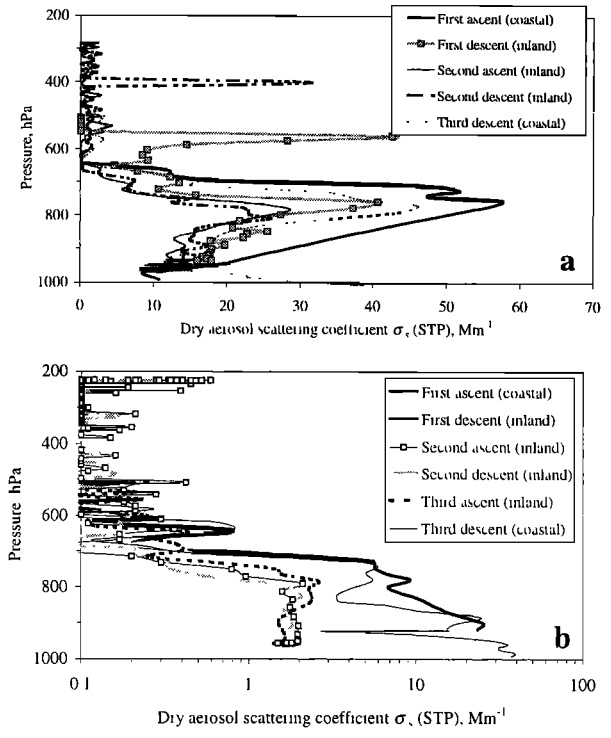

Figure 3. Selected vertical profiles of the aerosol particle scattering coefficient σ_s at 545 nm measured inland and offshore Suriname for (a) 25 March and (b) 26 March, 1998.

communication, 2000). Dry σ_s in the boundary layer were therefore converted to ambient conditions assuming that aerosols are mixed dust-sea salt (or sulfate), more hygroscopic than pure dust alone [*Li-Jones et al.*, 1998]. Following *Gassó et al* [2000], we set the scattering growth factor to 1.33 ± 0.07 at 80% RH.

On 25 and 26 March, vertical profiles of σ_s over Zanderij were measured between 1000 and 500 hPa. On these two days, ambient τ_s was 0.15 ± 0.02 and 0.050 ± 0.005 and accounted, respectively, for 48% and 38% of the extinction optical depth τ_a. The error on τ_s is calculated from the standard deviation of the scattering growth factor and the experimental error on the measured dry σ_s, assumed as independent variables. On 15 March, σ_s was measured from sea level up to 300 hPa (Figure 6). In this case, τ_s was 0.16 ± 0.02 and accounted for 50% of the ground-based τ_a (0.31 at 550 nm). This difference between τ_s and τ_a should not be attributed to the limited vertical coverage, as may be the case for 25 and 26 March, but both to the size cutoff of the inlet, which eliminates particles larger than 1 μm diameter, and to the contribution of absorption to column extinction. To estimate the effect of the inlet cutoff, we calculated the contribution of different particle size classes to τ_s using the column number size distribution $n_c(D_p)$ obtained from the spectral sky brightness measured at Zanderij. For spherical particles, the scattering optical depth τ_s is related to the aerosol column number size distribution by the Mie theory as

$$\tau_s(\lambda) = \int \pi \left(\frac{D_p}{2}\right)^2 Q_s(\lambda, D_p, \tilde{n}) n_c(D_p) dD_p$$

$$\sim \sum_i \pi \left(\frac{D_{p,i}}{2}\right)^2 Q_s(\lambda, D_{p,i}, \tilde{n}) n_c(D_{p,i}) dD_{p,i}, \quad (1)$$

where $Q_s(\lambda, D_p, \tilde{n})$ is the single-particle scattering efficiency. The integral is calculated as a discrete summation over the size range contributing to the number distribution (equation (1)), which in the actual case extended from 0.12 to 17 μm diameter (20 size class bins, parameterized by the i index). Analogous expressions are used to calculate the extinction and absorption optical depth (τ_a and τ_{abs}, respectively), given $Q_e(\lambda, D_p, \tilde{n})$ and $Q_a(\lambda, D_p, \tilde{n})$, the efficiencies of extinction and absorption as a function of particle size. The refractive index $\tilde{n}$ was set to $\tilde{n}$ = 1.55 - 0.005i, a value commonly used to estimate the optical properties of desert aerosols [*Moulin et al.*, 1997; *Formenti et al.*, 2000; *Schmid et al*, 2000]. Partial cumulative τ_s were calculated by adding progressively the contribution of each size class bin. Particles of diameter below 1–1.2 μm provided τ_s between 0.15 and 0.17, in agreement with the measured value. This accounted for between 43 and 48% of the τ_s from the whole particle distribution In comparison, the absorption optical depth τ_{ab} was estimated between 0 005 and 0.007, accounting for only 3% of the total extinction The errors on τ_s and τ_{ab} are ~35%, based on the expected uncertainties on the size distribution retrieval [*Dubovik et al*, 2000] We therefore attribute the discrepancy between the ground-based τ_a and the airborne derived τ_s to the truncation imposed by the inlet cutoff. As the size range obtained from the calculation is consistent with the upper size cutoff of the inlet, the calculation suggests that the sampling efficiency was excellent for particles below 1 μm diameter.

5.1.2. Considerations on the time evolution of the size distribution for mineral dust. The dust-laden air masses that reached the surface level in Suriname during March 1998 originated over the Moroccan desert and passed over the Canary Islands. In the case of the dust event that arrived in Suriname on 25–26 March, no comparison was possible between measurements in Suriname and those in Tenerife, because the layer generally remained below the elevation of our sampling site (Teide) in Tenerife (3570 m asl) Dust was, however, evident almost throughout March in the measurements performed at Izaña, at 2367 m asl (H. Maring, personal communication, 1999). The dust plume that arrived in Suriname on 15 March, was detected at Teide (Tenerife) on 7 March, where it caused an increase of τ_a at 500 nm from ~0.02 to 0.33. The Ångström exponent on this day was 0.20 ± 0.01, typical for Saharan dust [*Formenti et al.*, 2000]. When this air mass reached Suriname on 15 March, τ_a (measured at sea level) at 500 nm averaged 0.31 ± 0.02 and the Ångström exponent averaged 0.16 ± 0.07. As the

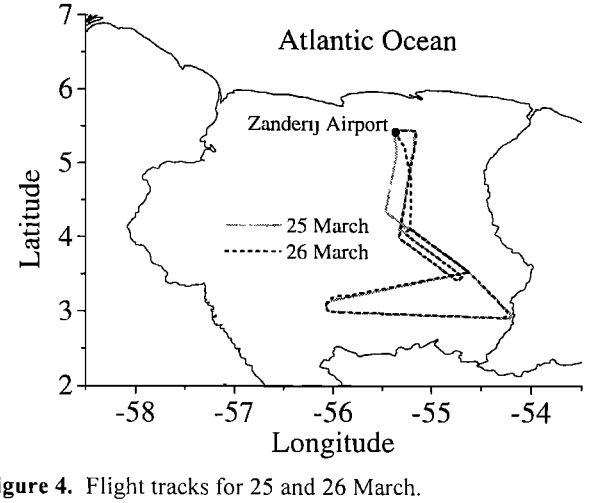

Figure 4. Flight tracks for 25 and 26 March.

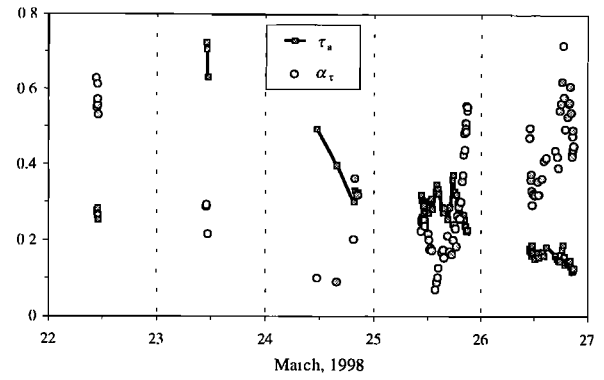

Figure 5. Time series of aerosol optical depth τ_a (500 nm) and of the Ångström exponent at Zanderij for the period 23–27 March.

Ångström exponents at the two sites were comparable, the size distributions should have similar shapes. The altitude of the site in Tenerife guarantees that mineral dust largely dominates the aerosol distribution during dust outbreaks, when the amounts of sea salt and pollution aerosols have been previously found to be negligible [*Patterson et al.*, 1977; *Formenti et al.*, 2000]. This is not the case for the surface site of Zanderij in Suriname, where concentrations of marine and pollution aerosols should be substantial. To estimate these contributions, for which no direct measurements are available, we used the three-mode number size distributions for sea salt and pollution (urban) aerosols published by *Jaenicke* [1998] The modal number density concentrations were adjusted in order to reproduce the maximum amount of marine and pollution aerosols expected on the basis of the bulk filter measurements at Zanderij. Cl was used as the unique tracer for sea salt. Na is also a major component of sea-salt aerosols, but it is present in significant amounts in mineral dust. Pollution was traced with non-sea-salt S (measured S minus S from sea salt). The contribution of atmospheric dimethyl sulfide (DMS) to the S concentrations, which we could not quantify directly, was assumed as 0.1 μg m^{-3} in the fine fraction based on the measurements of *Li-Jones and Prospero* [1998] at Barbados. This accounted for 9% of the maximum measured fine S. Coarse S was left uncorrected. Maximum S concentrations coincided with the highest reading of fine BC (4 μg m^{-3}), confirming S to be well representative of pollution aerosols. In both cases the vertical distributions were assumed to be decreasing exponentially with height within the boundary layer below 2 km

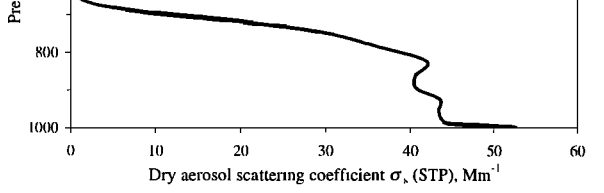

Figure 6. Vertical profile of the aerosol particle scattering coefficient σ_s at 545 nm over Zanderij for 15 March 1998. The dust layer is evident up to 700 hPa.

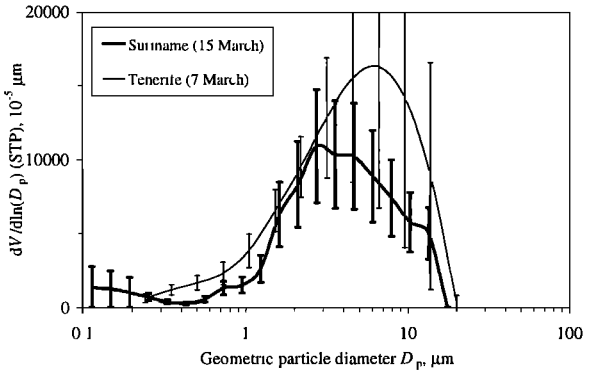

Figure 7. Column aerosol volume distributions $dV/d\ln(D_p)$ (STP) retrieved at Mount Teide on 7 March 1998 and at Zanderij on 15 March 1998. Error bars are the computational uncertainties on the retrieval.

with a height scale factor of 900 m [*Jaenicke*, 1993]. The size-dependent corrections derived for the column volume distribution at Zanderij averaged 32 ± 18% between 0.2 and 1 μm diameter and 12 ± 4% between 1 and 14 μm diameter. We limited the calculation to these size intervals as the uncertainty on the retrieval of the volume distribution exceeds 35% outside these boundaries [*Dubovik et al*, 2000].

As the settling velocity depends on the particle size, the shape of the size distribution should evolve according to the differential efficiency of removal. In Figure 7 the STP volume distributions per unit column of air $dV/d\ln(D_p)$ retrieved at Teide and in Suriname (corrected) are shown. Despite the large computational uncertainties affecting both distributions, we can derive some indications about the mechanism that regulated the evolution of the size distribution at Teide into the one at Zanderij. For a given particle size, the evolution of the number concentration N as a function of time is described by the equation

$$N(t) = N_0 e^{-t/\tau}, \tag{2}$$

where N_0 is the number concentration at time $t = 0$, and τ is the particle lifetime in the atmosphere. The major mechanisms of particle removal are dry deposition via gravitational settling and wet deposition via rain washout; both define a particle atmospheric lifetime, which we indicate as τ_{dry} and τ_{wet}, respectively. An empirical expression of the size-dependent residence time of an aerosol particle has been given by *Jaenicke* [1998] as

$$\frac{1}{\tau} = \frac{1}{\tau_{dry}} + \frac{1}{\tau_{wet}}$$

$$= \frac{1}{1.28\times10^{8}}\left(\frac{D_p}{0.6}\right)^{2} + \frac{1}{1.28\times10^{8}}\left(\frac{D_p}{0.6}\right)^{-2} + \frac{1}{\tau_{wet}}, \tag{3}$$

The residence time $1/\tau_{dry}$ depends on particle diameter D_p. We have plotted in Figure 8 the ratio $N(t)/N_0$ obtained from the retrieved size distributions: $N(t)$ is the particle number concentration at Zanderij, while N_0 is the particle number concentration at Teide. Correspondingly, we have plotted the ratio calculated as $\exp(-t/\tau)$ for a time interval t of 8 days, assuming as a first approximation dry deposition only, that is, $\tau =$

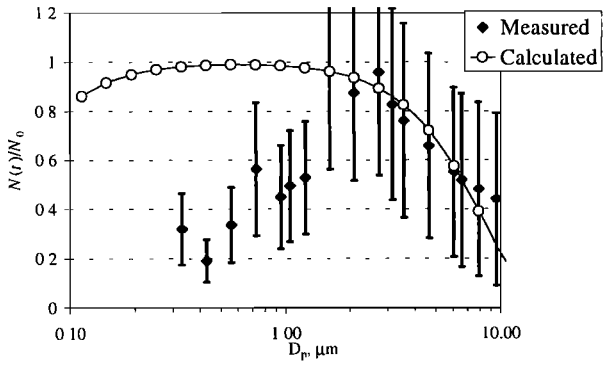

Figure 8. The size-dependent removal rate $N(t)/N_0$ obtained for the column aerosol size distributions retrieved at Mount Teide on 7 March 1998 (N_0) and at Zanderij on 15 March 1998 ($N(t)$) is compared to the removal rate obtained assuming dry deposition only Gravitational settling is sufficient to explain the depletion for particles larger than 1.6 µm diameter, but not for particles smaller than 1.6 µm diameter, for which additional removal via wet deposition has to be assumed. Error bars are computed from the retrieval uncertainties on the volume distributions.

τ_{dry}. Results in Figure 8 show that for large particles (1.6–10 µm diameter) depletion can be accounted for assuming gravitational settling only. Error bars are large and limit more quantitative conclusions. For particles between 0.3 and 1.6 µm diameter, wet deposition is necessary in addition to explain the observed $N(t)/N_0$ ratio, which is below 60%. The size bins outside the interval 0 3–10 µm were excluded from the calculation because their uncertainties exceeded 80%

5.2. Chemical Observations

Aerosol samples taken at Zanderij on 24, 25, and 26 March showed the contribution of sea salt and mineral dust: The presence of sea salt was traced by the coarse Cl/Na mass ratio, which was 1.84 ± 0.05 (the ratio expected in sea salt is 1.81 [*Riley and Chester*, 1971]); mineral dust was traced by the coarse Si/Al ratio, equal to 2.4 ± 0 7, as previously reported for Saharan/Sahelian dust [*Chiapello et al*, 1997]. Discussion of the elemental ratios for mineral dust is given in section 6 1. Al, Si, Ca, Ti, Mn, and Fe were attributed to mineral dust. K was generally also associated with mineral dust (coarse K/Al mass ratio 0.3–0.6), except on the night of 26–27 March, when K/Al was equal to 34 in the fine fraction and 7 in the coarse fraction. *Chiapello et al.* [1997] have shown that the ratio K/Al is highly variable in the mineral dust from Africa and might range from 0.7 to 4.8; the enrichment of K in the fine fraction exceeds this variability and suggest that this sample might be unreliable. K may also derive from biomass burning [*Gaudichet et al.*, 1995]. *Andreae* [1983] used the mass ratio of excess-fine K to fine BCE as an indicator of the presence and age of biomass burning plumes. Excess-fine K is obtained by subtracting from the measured fine K the fraction due to soil dust and sea salt. The soil fraction was estimated from the measured fine Al using the mass ratio K-to-Al of 0.32 in average crustal rock [*Mason*, 1966]. The use of the Mason' s model as a crustal reference material can be questioned, because the elemental ratios in airborne soil dust (and particularly Saharan dust) might be very different from average crustal rock, as is evident from the data of *Chiapello et al* [1997] and will be shown in the following discussion. Using a well-established standard reference model like *Mason* [1966] eliminates, however, the ambiguities inherent to changes in soil composition (for example in the transition from background to dust-loaded conditions, section 6.2), and it is advantageous for comparison purposes. The contribution of sea salt to fine K was estimated from Cl in the fine aerosol and the K to Cl ratio in seawater (0.021 [*Riley and Chester*, 1971]).

Fresh smoke aerosols have values of excess-fine K to fine BCE (by mass) of 0.26–0.36, while in Sahara dust plumes the ratio is 0.10–0.16 [*Andreae*, 1983]. In our samples the ratio excess-fine K to fine BCE ranged from 0.01 to 0.13. On the night of 26–27 March maximum concentrations for FPM, fine BCE, fine Na, S, Cl, Cu, and Br were measured. The enhancement of Na, Cl, and S suggests the influence of maritime air, while that of fine BCE and fine Cu suggests mixing with anthropogenic pollution. This is also evident in the increase of the mass ratio of fine V/Al from ~ 0.002–0.003 (typical of mineral dust [*Mason*, 1966]) to 0 013. V is a good tracer of anthropogenic pollution, as it is emitted during residual oil combustion [*Chow*, 1995]. Ten-day back trajectories for the sample from 26–27 March showed northeasterly flow at all pressure levels: Below 850 hPa air masses originated over the southern United States, but recirculated over the ocean for more than 5 days, indicating that the low troposphere was impacted by aged anthropogenic pollution transported within maritime air masses and mixed with mineral dust aerosols.

Samples were also collected at the forest site of Sipaliwini on 23, 25, and 26 March. Here the contribution of sea salt was less important (coarse Cl/Na mass ratio of around 0.6). Mineral dust was evident from a coarse Si/Al ratio around of 1.6. Ca, Ti, Mn, V, and K showed ratios typically associated with mineral dust The ratio K/Al was generally around 0.4–0.7 in both size fractions. The ratio of excess-fine K to fine BCE ranged from 0 05 to 0.10, which excludes any major influence of biomass burning. In contrast to the coastal site, where P was always below the detection limit, P was constantly detected at the forest site, with concentrations between 11 and 67 ng m^{-3} in the coarse fraction. P is a biogenic component emitted mainly during plant guttation and transpiration [*Artaxo and Hansson*, 1995].

6. Observations in Brazil

At Balbina, transport of mineral dust from Africa within the NE trade winds took place without interruption from 24 to 27 March. According to the back trajectories, the source region of air masses was generally the Moroccan coast for trajectories arriving below 800 hPa, and the Sahel area for those arriving at higher levels. Bursts of mineral dust in the Central Amazon Basin have been observed previously [*Talbot et al.*, 1986; *Swap et al.*, 1992]. Dust is transported across the North Atlantic Ocean within undisturbed layers in steady state below 700 hPa (as shown by the nephelometer vertical observations over Suriname). *Swap et al* [1992] have demonstrated that dust is transported across the ITCZ into the Southern Hemisphere by synoptic scale systems, in contrast with the common idea of depletion via wet removal of such plumes. Precipitation was also observed at Balbina during the dust outbreak, on 26 March.

During the period 30 March–13 April, 10-day back trajectories showed that air masses arriving at the surface level at Balbina traveled from the eastern coastline almost in parallel with the Amazon River. Several populated centers, as well as industrial and agricultural activities are located in this region, particularly

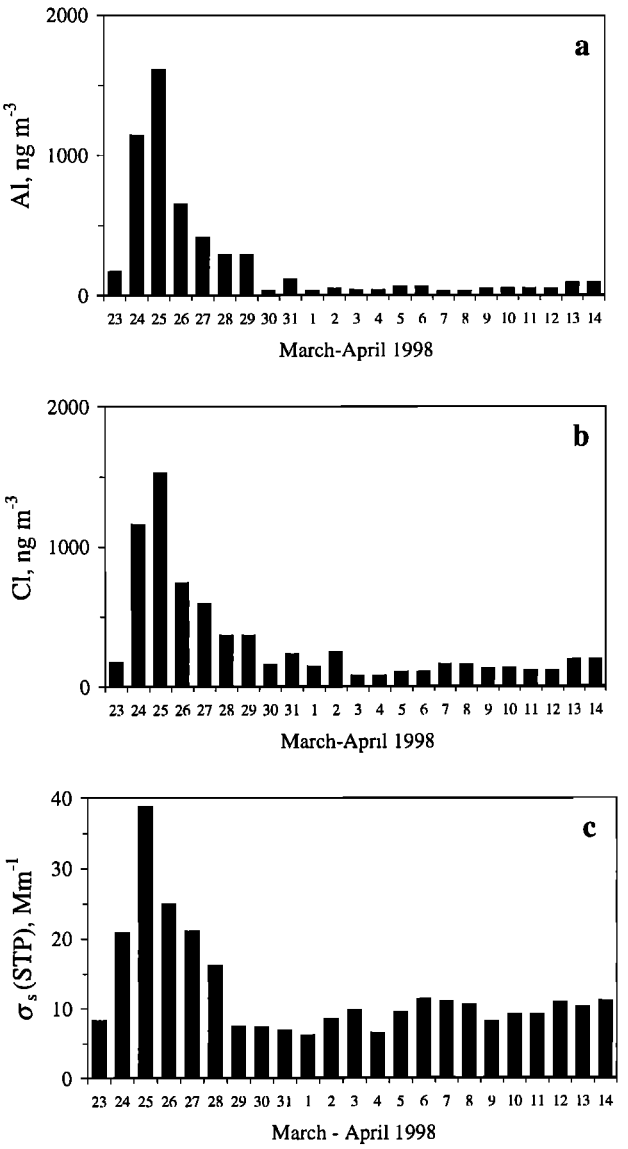

Figure 9. Time series of coarse (a) Al and (b) Cl and (c) σ_s measured at Balbina from 23 March to 14 April 1998.

along the coast. On 5, 8, and 13 April, air masses originated over the Atlantic Ocean. We therefore expect both marine and continental aerosols to influence the aerosol composition at Balbina. Figure 9 shows the time series of coarse Al and Cl (Figures 9a and 9b) and σ_s (Figure 9c). The distinction between the period 30 March–13 April and the period 24–27 March is clear. Analogous behavior was observed for TSP, FPM, CPM, fine and coarse BC and the major elements (Na, Mg, K, Ca, Ti, V, Mn, Fe, Zn, and Sr) in both size fractions. Between 24 and 26 March, the PM_{10} mass (PM_{10} mass is the sum of FPM and CPM) and the PM_{10} Si concentrations increased from 7 ± 1 and 0.12 ± 0.05 μg m^{-3} (respective mean concentrations during 30 March to 13 April) to 26 ± 7 and 7.5 ± 0.7 μg m^{-3}. Values for σ_s increased from 10 ± 1 Mm^{-1} (mean background value) to 26 ± 8 Mm^{-1} (24–26 March mean). Coarse P and OC did not show any evidence of the occurrence of dust (Figure 10). These elements are emitted as primary aerosol from the rain forest [*Artaxo et al.*, 1990].

6.1. Chemical Composition

In Table 1 the mean concentrations measured in the fine fraction during the background (30 March to 13 April) and the dusty (24–26 March) periods of CLAIRE-98 are compared to the results of the Atmospheric Boundary Layer Experiment (ABLE) 2A and ABLE 2B, measured at a site about 100 km from Balbina [*Artaxo et al.*, 1988; 1990]. ABLE 2A was conducted during the dry, biomass burning season, and ABLE 2B during the wet season, that is, under pristine conditions more directly comparable to the CLAIRE-98 situation. The results from ABLE 2A, on the other hand, provide upper limit concentrations to our experimental findings.

6.1.1. Tracers of biogenic emissions. P, S, K, Cu, and Zn originate from biogenic emissions from the rain forest [*Artaxo et al*, 1990]. When vegetation burning occurs, the concentrations of these elements are enhanced in the fine fraction, with the exception of P, which is mainly emitted in the coarse fraction [*Gaudichet et al.*, 1995]. During the background period of CLAIRE-98, concentrations of P, S, K, Cu, and Zn resembled the values measured during ABLE 2B. Coarse P averaged 33 ± 9 ng m^{-3}, in the range observed at Sipaliwini. The coarse P background values were as high as during the dust episode, indicating that coarse P was generated locally (from forest emissions) and not transported within the Saharan dust layer. Analogous findings applied to total OC. The percentage of organic material transported within the Saharan dust plumes is only of the order of 3% [*Li et al.*, 1996; *Prospero*, 1999]. Values of S, K and Zn were lower than during ABLE 2A, which took place during the biomass burning season. In both size fractions, P, S, K, Cu, and Zn were enriched with respect to their ratios to Al in average crustal rock [*Mason*, 1966], which confirms the contribution of vegetation emissions. The S budget is discussed below. No striking indications of enrichment in the fine size fraction were found in the measured mass size distributions of these elements (not shown), thus excluding an enhancement due to forest fire emissions. The mass ratio excess-fine K to fine BCE was 0.10 ± 0.02, in line with the previous conclusion.

6.1.2. Tracers of sea salt emissions. Na and Cl are the major elements in sea salt. Na is also a significant element in soils, while Cl is emitted during plant transpiration [*Nemeruyk*, 1970] and vegetation fires [*Gaudichet et al.*, 1995; *Andreae et al.*, 1998]. Evidence of biogenically derived Cl in the Amazon forest has been presented previously [*Artaxo et al.*, 1990]. While the CLAIRE background concentrations of fine Na (26 ± 20 ng m^{-3}) are lower but comparable to those of ABLE 2B, mean background fine Cl (65 ± 33 ng m^{-3}) was 7 to 10 times higher than the means for ABLE 2A and 2B. Concentrations of water-soluble Cl^- up to 74 ng m^{-3} in the forest boundary layer above the Guyanas have been reported by *Gregory et al* [1986]. *Echalar et al.* [1998] reported mean Cl concentrations of 67 ± 75 ng m^{-3} (fine) and 58 ± 75 ng m^{-3} (coarse) for the dry season at Alta Floresta, a site at almost the same longitude as Balbina. In the latter case, however, Cl emissions were certainly due to forest fires. In addition to plant transpiration, the excess Cl concentrations in the Amazon basin have been previously attributed to transport of sea-salt aerosol embedded in dust plumes transported at low altitude [*Talbot et al*, 1986; *Swap et al.*, 1992; *Artaxo et al.*, 1995]. This was also observed in Balbina by looking at the correlation between Na and Cl. During the background period, Na and Cl were correlated in the coarse fraction (r^2 = 0.72) but less in the fine fraction (r^2 = 0.37). The correlation increased significantly when the data corresponding to the dust episode were included: By doing so, the coefficients of correlation were r^2 = 0.99 (coarse) and r^2 = 0.75 (fine). Transport from the coastline was more direct during the dusty period. During background conditions only, the mass ratio of Cl-to-Na

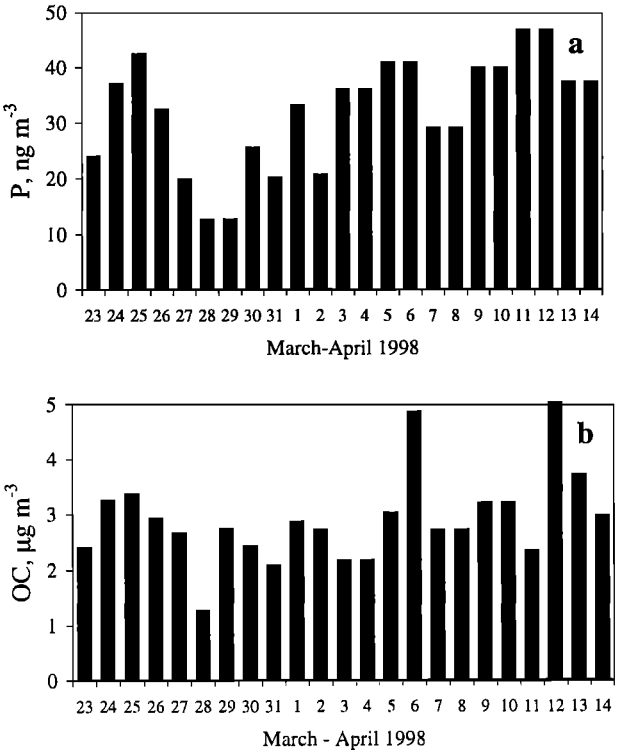

Figure 10. Time series of (a) coarse P and (b) organic carbon (OC) measured at Balbina from 23 March to 14 April 1998.

approximated the sea-salt value (1.81) when coarse Na > 40 ng m^{-3}. Below 40 ng m^{-3}, Cl showed significant enrichment (a factor of 4 to 7) with respect to Na. The Cl-to-Na ratio further increases after correcting Na and Cl for their soil dust component. The correction is of the order of 7–18% for Na [*Maenhaut et al.*, 1996b], but only of the order of 0.2% for Cl. We conclude that maritime air affected the site (as confirmed by 10-day back trajectories) and significantly contributed to the concentrations of Cl. Excess Cl, particularly in the fine size fraction, was likely due to biogenic emissions from the vegetation of the rain forest.

6.1.3. Tracers of anthropogenic emissions and S budget. Concentrations of elements related to anthropogenic activities (S, V, Ni, Cr, Pb, and Br) [*Chow*, 1995] were either below their detection limit (Ni, Cr, and Pb) or very low (S, V, and Br). In the fine fraction, where most of the anthropogenic emissions are expected, S was enriched (by 3 orders of magnitude) with respect to its ratio to Al in average crustal rock [*Mason*, 1966], as well as with respect to Na from sea salt (a factor of 40). Previous studies have shown that background sulfate concentrations over the Amazon can be only partially explained by biogenic emission of several sulfur-containing gases (DMS, H_2S, etc.) from the vegetation [*Andreae et al*, 1988; 1990; *Artaxo and Hansson*, 1995]. During ABLE 2B the contribution of biogenic emissions was minor with respect to that of marine and anthropogenic emissions, which together accounted for up to 90% of measured sulfate aerosols [*Andreae et al*, 1990]. Lack of appropriate tracers does not allow us to quantify the anthropogenic component, but based on the low EC concentrations (< 10 ng m^{-3}), we estimate that during CLAIRE-98 anthropogenic pollution made only a minor contribution to sulfate aerosols. We propose that sulfur concentrations measured at Balbina were mainly due to maritime inputs. In particular, because the S-to-Na mass ratio is highly enriched with respect to sea salt, we suggest that oxidation of marine DMS was the primary contributor.

6.1.4. Tracers of dust emissions. During the background period of CLAIRE-98, concentrations of the mineral dust elements (Al, Si, Ca, Ti, Mn, and Fe) were even lower than observed during ABLE 2B. Wind erosion is minimal on the weathered soils in the Amazon during the rain season; therefore such low concentrations are not surprising. The effect of the dust event on these elements was major. Concentrations measured between 24 and 26 March were at least an order of magnitude higher than the mean background (Table 1).

In both size fractions, elemental mass ratios of Si, Ca, Ti, Mn, and Fe with respect to Al resembled the ratios in average crustal rock [*Mason*, 1966]. Ratios for Si were 2.1 ± 0.3 in the fine and 1.3 ± 0.3 in the coarse fraction. Some elemental ratios with respect to Al and Ca are reported in Table 2 for the fine and coarse fractions, for both dust and nondust conditions. Results for Balbina are compared with analogous quantities obtained during the same days at Zanderij and at Sde Boker, in Israel, which also was affected by Saharan dust. At Sde Boker the PM_{10} concentration (sum of FPM and CPM) reached 0.8 mg m^{-3} on 15–16 March, far above the long-term (1995–1998) average, which is of the order of 50 µg m^{-3}. Assuming dust to be uniformly distributed in a 5 km deep layer, the 15–16 March average is consistent with the MEDUSE predictions (dust atmospheric concentration of 1 mg m^{-3}). In addition, σ_s increased from 63 ± 15 Mm^{-1} (mean background over the period 1–14 March) to 900 ± 1000 Mm^{-1} (daily average during 16 March; maximum recorded σ_s 3261 Mm^{-1}).

In Table 2, results for Balbina, Zanderij, and Sde Boker are compared to the corresponding elemental ratios obtained by *Chiapello et al* [1997] for dust outbreaks at the Cape Verde Islands, 500 km downwind of the Sahara/Sahel basin. *Chiapello et al.* [1997] used these elemental ratios to distinguish different dust source regions (Sahel, north central Africa, and northwest Africa). A certain homogeneity is observed in the Si and Ca ratios to Al at the three sites both under dust and dust-free conditions, with the exception of Israel, where the local soil is highly calcareous [*Foner and Ganor*, 1992]. Our values are consistent with the estimates of *Chiapello et al* [1997], and would suggest the Sahel as the source region of the mineral dust transported to Balbina and Suriname. This conclusion, however, is not supported by the air mass back trajectories. Both the KNMI and the HYSPLIT4 models (using independent input wind fields; ECMWF and NCEP FNL for KNMI and HYSPLIT4, respectively) indicated that air masses at surface level originated over northern Africa (Morocco) rather than over the Sahel. However, the confidence in the trajectory calculations becomes low when transport is long (i.e., for time intervals longer than 5 days). To verify whether divergence of the airflow as a function of transport time would affect our results, a test on the HYSPLIT4 calculations was performed using clusters of five back trajectories with starting points at latitudes and longitudes 1° apart, with the centroid at Balbina. With the exception, in one case, of the southernmost trajectory, divergence was minimal at all pressure levels, including at the surface. Although probably not conclusive, this test gives some confidence in the determination of the air mass source region.

At the three sites, the P-to-Al ratio during the dusty periods approached the average value (0.042 ± 0.007) measured for Saharan dust by *Bergametti et al.* [1989] at Fuerteventura (Canary Islands). Outside the dust episodes, the P-to-Al ratio was higher. However P measured at Balbina is attributed almost entirely to aerosol from the vegetation, and differences in the P-

Table 1. Mean Concentrations for Particle Mass (PM) and Various Elements in the Fine and Coarse fraction at Balbina

	Balbina Coarse		Balbina Fine		ABLE 2A	ABLE 2B
	Background	Dusty Period	Background	Dusty Period	Fine	Fine
Na	54	657	26	268	—	49
Mg	—	252	—	126	12	23
Al	56	1135	23	692	8	62
Si	67	2099	48	1428	—	156
P	33	37	5	13	4	6
S	32	144	68	231	259	83
Cl	155	1143	65	181	6	10
K	69	264	18	195	161	32
Ca	11	282	5	115	4	11
Ti	4	72	1.5	46	0.9	5
V	0.07	1.4	0.10	1.03	1.1	0.5
Cr	—	—	—	—	0.8	5
Mn	0.4	9.6	0.22	5.5	0.3	0 9
Fe	25	536	12	344	6.5	37
Ni	—	—	—	—	0.5	0.3
Cu	0.2	—	0.2	0.46	0.4	0.2
Zn	0.6	1.9	0.25	1.6	1.6	0.7
Br	1.8	3.4	0.58	—	1	0.6
Pb	—	—	—	—	0.7	0.6
PM	5.8	17.9	1.6	8.4	6.7	1.8
OC	2.5	1.0	0.77	2.2		
EC	0.08	0.2	0.10	0.7		

Concentrations are expressed in ng m^{-3}, except for PM, organic carbon (OC) and elemental carbon (EC), for which they are in μg m^{-3}. Averages are calculated during (24–26 March) and outside (30 March–13 April) the dust episode. For comparison, the fine elemental concentrations measured at a nearby site during the Atmospheric Boundary Layer Experiment (ABLE) 2A (dry season) and ABLE 2B (wet season) [*Artaxo et al.*, 1988; 1990] are also presented.

to-Al ratio between dusty and nondusty periods are not significant.

6.2. Mass Size Distributions

The mass size distributions $dM/d\log(EAD)$ of several particulate elements (Al, P, S, Cl, K, Ca, V, and Zn) are shown in Figure 11 for dust (25 March) and background (3 April) conditions. Generally, the effect of the Saharan plumes is seen as an enhancement of the coarse mode concentrations, although the overall shape of the mass distributions is preserved. Al, Cl, K, and Ca (but also Ti and Fe, not shown) show single-mode distributions centered at 2–3 μm EAD, typical of soil and sea-salt elements. An additional fine mode at 0.3 μm EAD is evident for K during dust conditions. Zn has similar behavior to K. The plot of K/Al as a function of particle diameter for the two selected days (Figure 12) provides the rationale for the use of *Mason* [1966] instead of actual data as the crustal reference model to correct the measured K concentrations for the soil component (section 5.2 and following). The ratio between these two elements is highly variable and depends on both the aerosol type and size. As a consequence the selection of a reference ratio based on experimental data would be in any case arbitrary and prone to substantial uncertainty.

The mass size distribution for P also shows a coarse mode around 2-3 μm EAD, which was not substantially modified, in magnitude or shape, by the presence of dust.

S shows bimodal mass size distributions with a fine mode centered at 0.2–0.3 μm EAD and a coarse mode around 2–3 μm EAD. The enhancement during the dust event is attributed to marine/DMS aerosols transported to the site together with the dust plume.

V, Cr, and Ni showed a single-mode distribution centered around 2 μm EAD during dust conditions, while they were below the detection limit during the background period.

6.3. Mass Apportionment

Chemical mass balance (CMB) apportionment [*Gordon*, 1988] was done separately for the coarse and fine size fractions considering three source profiles: (1) mineral dust, which was traced by Al, Ti, and Fe proportioned according to the average crustal rock of *Mason* [1966]; (2) sea salt, for which Na was chosen as a tracer assuming the sea-salt composition from *Riley*

Table 2. Elemental Ratios for Some Elements at Balbina, Zanderij, and Sde Boker During Dusty Periods and Background Conditions (in Parentheses)

	This Study			*Mason* [1966]	*Chiapello et al.* [1997]		
	Balbina	Zanderij	Sde Boker	Crustal Rock	Sahel	South Mid Sahara	Northwest Sahara
			Fine Fraction				
Si/Al	2.0 ± 0.1 (2.1 ± 0.3)	1.9 (2.75)	2.3 (2.5 ± 0 2)	3.4	2.03	2.21	2.32
Ca/Al	0.16 ± 0.01 (0.24 ± 0.04)	0.13 (0.17)	1.9 (4.5 ± 1.2)	0.5	0.20	0.36	0.60
P/Al	0 011 ± 0.001 (0 26 ± 0.10)	0.04 (0.26)	0.22 (0.7 ± 0 4)	0.013	—	—	—
K/Ca	1.6 ± 0.1 (3.7 ± 1.1)	3.2 (5.7)	0.11 (0.3 ± 0.2)	0.7	0.96	0.62	0.43
Fe/Ca	3.04 ± 0.01 (2.2 ± 0.4)	3.5 (2.9)	0.34 (0.21 ± 0.06)	1.4	2 71	1.43	0.90
			Coarse Fraction				
Si/Al	1.87 ± 0.06 (1 3 ± 0.3)	1.7 (2.2)	1.8 (2.2 ± 0.1)	3.4	2.03	2.21	2.32
Ca/Al	0.26 ± 0 03 (0.22 ± 0.09)	0.25 (0 65)	2.0 (6.1 ± 1.1)	0.5	0.20	0.36	0.60
P/Al	0.04 ± 0 01 [b] (0.7 ± 0.32)	0.11 (1.34)	0 03 (0.5 ± 0.5)	0.013	—	—	—
K/Ca	0.7 ± 0 2 (7 0 ± 3.0)	1.5 (5.0)	0.11 (0 07 ± 0.02)	0.7	0.96	0.62	0.43
Fe/Ca	1 8 ± 0.2 (2.3 ± 0 7)	1 6 (0.7)	0 32 (0.13 ± 0 03)	1 4	2 71	1.43	0.90

[a] For comparison, the elemental ratios obtained by *Chiapello et al* [1997] for dust outbreaks at the Cape Verde Islands, 500 km downwind the Sahara, and ratios for the average crust composition [*Mason*, 1966], are presented.
[b] P not corrected for background.

and Chester [1971], and (3) excess sulfate, which was apportioned by assuming that excess S (i.e., residual S concentrations after correction for the sea-salt component) was present as pure sulfate ($S/SO_4^{2-} = 0.334$). Excess sulfate accounts for the contributions of distant sources such as marine DMS oxidation and anthropogenic pollution, as well as for that of biogenic emission from the rain forest. Unfortunately we are unable to separate these contributions.

The apportionment results for the fine and coarse size fractions (i.e., the concentrations in $\mu g\ m^{-3}$ for each aerosol type in the two fractions) were summed up for each sample to obtain the apportionment for the PM_{10} fraction (PM_{10} denotes the sum of FPM and CPM). The CMB apportionment was complemented with data for organic aerosol, which we estimated from the measured OC concentrations as 1 5 OC [*Seinfeld and Pandis*, 1997]. Results are shown in Figure 13. In general, the PM_{10} mass was reproduced within 20%, overestimated during the dust period, but underestimated during the background period. Mineral dust contributed on average 70% of the mass during the dusty period, and only 20% otherwise. Organic aerosols dominated the PM_{10} mass (contribution of the order of 50–70%) during the background period, while their contribution remained within 30% between 24 and 27 March. The absolute contribution of organic aerosols was rather constant (~3 $\mu g\ m^{-3}$), confirming that organic carbon was predominantly derived from the rain forest. Sulfate aerosols accounted in average for only 5% of the mass

An alternative mass apportionment (not shown) was performed by calculating the crustal matter mass from measured PM_{10} concentrations as

$$\text{crustal matter} = 1.16\,(1.90\,\text{Al} + 2.15\,\text{Si} + 1.41\,\text{Ca} + 1.67\,\text{Ti} + 1.48\,\text{Fe}), \quad (4)$$

This model assumes the major soil elements Al, Si, Ca, Ti, and Fe to be present in soil dust as oxides in the form of Al_2O_3, SiO_2, CaO, TiO_2, and Fe_2O_3. In the model, CaO is used instead of $CaCO_3$ owing to the differences in the Ca/Al ratios (Table 2) between Balbina and Sde Boker, where the soil dust is dominated by calcium carbonate [*Formenti et al*, 2001]. The factor 1.16 takes into account the missing contributions of MgO, Na_2O, K_2O, and H_2O. With this choice the uncertainties related to the apportionment of Na and K into their soil and nonsoil components (see previous sections) are bypassed.

Using this model, the contribution of mineral dust to the total mass was lower, between 50 and 60% during the dust event and below 8% otherwise. The missing mass (between 10 and 20%, needed to reproduce the experimental mass within 10%) could be compensated by increasing the amount of organic matter, that is,

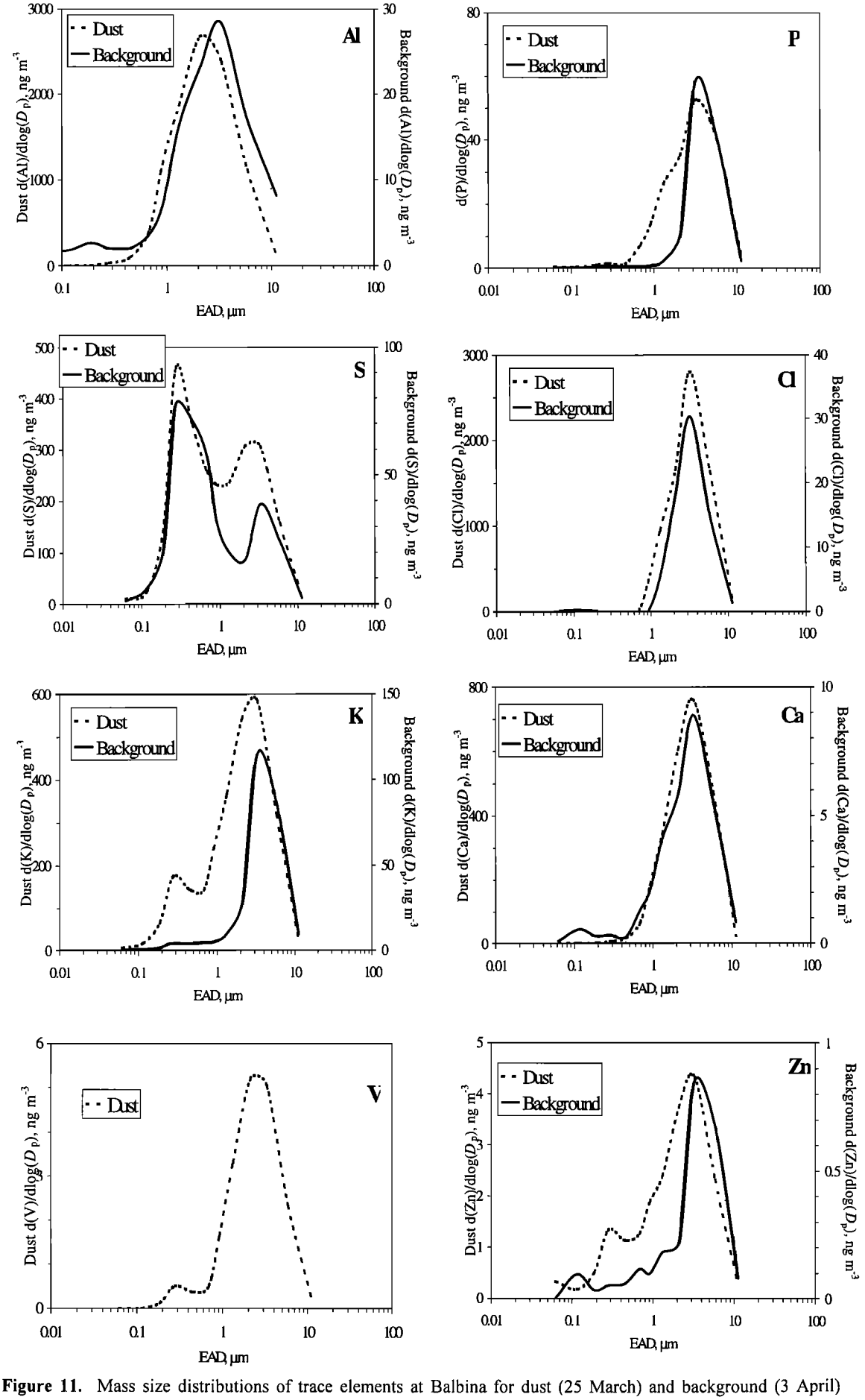

Figure 11. Mass size distributions of trace elements at Balbina for dust (25 March) and background (3 April) conditions

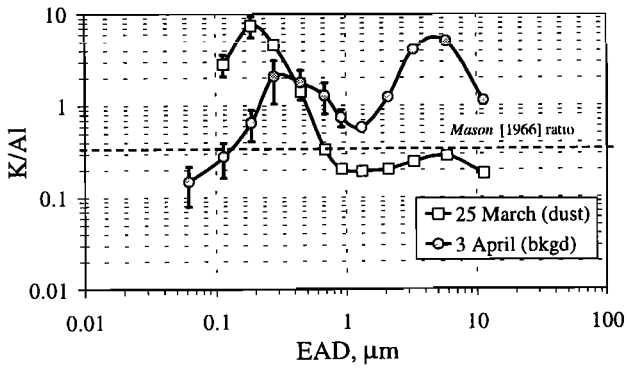

Figure 12. K/Al mass ratio as a function of particle aerodynamic diameter obtained from the measurements of the mass size distributions at Balbina for dust (25 March) and background (3 April) conditions. The K/Al ratio in average crustal rock of *Mason* [1966] is shown for comparison.

by setting the conversion factor between organic aerosol and organic carbon to 1.9–2.0. With this choice, organic aerosols account for up to 90% of the mass during background periods. In the previous CMB calculation, the conversion factor was set to 1 5 based on the discussion of *Seinfeld and Pandis* [1997] and on available measurements (see references therein). *Turpin et al.* [2000] have recently reviewed the estimate of organic matter from measurements of organic carbon and suggested that in nonurban areas the higher percent contribution of primary biogenic organic aerosols would result in a higher average organic molecular weight per carbon weight, and therefore in a higher conversion factor Our results support the same conclusion However, because they are based on a rather arbitrary adjustment of the organic matter mass in order to reproduce the gravimetric PM_{10} mass within its experimental error (~10% or lower), we cannot consider our results as conclusive. The use of either crustal model is almost equivalent when considering the uncertainties associated with the working hypothesis.

6.4. Optical Properties

The mean background ambient σ_s at Balbina was 10 ± 1 Mm^{-1} To convert the σ_s values from ambient to dry conditions, we estimated a scattering growth factor from the mean geometric growth factor measured at Balbina for submicrometer diameter particles (six size classes between 35 and 264 nm dry diameter) (E. Swietlicki et al., manuscript in preparation, 2000). The geometric growth factor was measured between RH < 10% and RH around 90%. The aerosol size distributions measured for the submicrometer fraction for pristine wet conditions were essentially unimodal with geometric growth factors between 1.1 and 1.4, corresponding to organic material (E. Swietlicki et al., manuscript in preparation, 2000). For submicrometer particles, for which the scattering efficiency $Q_s(\lambda,D_p,\tilde{n})$ can be approximated as ~ kD_p (k is a constant), the scattering and the geometric growth factors are related as

$$\frac{\sigma_s(RH)}{\sigma_s(dry)}=\left(\frac{D_p(RH)}{D_p(dry)}\right)^3, \quad (5)$$

where dry and RH refer to two fixed values of relative humidity corresponding to dry and hydrated conditions. The scattering growth factor therefore ranges between 1.3 and 2.7 and the mean dry background σ_s ranges between 5 ± 1 Mm^{-1} and 8 ± 1 Mm^{-1}. The absorption coefficient σ_a (assumed as humidity independent) at 550 nm averaged 0.4 ± 0.1 Mm^{-1}. The single scattering albedo ω_0 at 550 nm ($\omega_0 = \sigma_s/(\sigma_s + \sigma_a)$) averaged 0.96 ± 0.01 at ambient conditions. The corresponding dry ω_0 varied between 0.92 ± 0.01 and 0 95 ± 0.01. For comparison, the maximum mean dry ω_0 reported for biomass burning aerosols during Smoke, Clouds, and Radiation-Brazil (SCAR-B) was 0.87 ± 0.05 [*Reid and Hobbs*, 1998; *Reid et al.*, 1998], while over the east coast of the United States, a source region of anthropogenic industrial pollution, mean dry ω_0 was estimated as 0 90 ± 0 06 [*Hegg et al*, 1997].

Increased σ_s correlated with the mineral dust event. This is shown in Figure 14 by the linear regression of σ_s against Al_f, Al_c and $Al_{PM_{10}}$ (Al concentrations in the fine, coarse, and sum of both size fractions, respectively), chosen as independent variables. The square of the correlation coefficient was r^2 = 0 67–0 71.

During the dust event the σ_s were considered as dry values as the relative humidity remained mostly below 60% during daytime and below 75% during nighttime. For a scattering growth factor of 1.3 at 80% RH [*Gassó et al*, 2000], the error introduced by this assumption is within 30%.

The slope of the linear regression between σ_s and Al corresponds to the Al mass scattering efficiency (α_{Al}). Knowing the soil-to-Al mass ratio, α_{Al} can be converted into the dry mass scattering efficiency for soil dust (α_{dust}). Al concentrations account for 7.1% to 8.2% of the soil composition according to *Artaxo et al.* [1990] and references therein, or for 6% to 8% according to *Taylor and McLennan* [1985]. Therefore lower and upper limits of α_{dust} were estimated from the Al mass scattering efficiency α_{Al} multiplied by 6% (lower α_{dust}) and 8.2% (upper α_{dust}). The overall variability between lower and upper α_{dust} is 37%. The resulting mass scattering efficiency α_{dust} was (1) 1.8 (± 0 2) – 2.4 (± 0.2) $m^2\ g^{-1}$ in the fine fraction; (2) 1.1 (± 0.1) – 1.5 (± 0.2) $m^2\ g^{-1}$ in the coarse fraction; and (3) 0.67 (± 0.07) – 0.91 (± 0.09) $m^2\ g^{-1}$ for PM_{10} soil dust. Errors in parentheses are fitting uncertainties only. The intercept of the each regression line was around 8 Mm^{-1}, corresponding to the upper limit of the σ_s background average. When using as independent variables the values of soil mass estimated in section 6.3 using (1) CMB and (2) equation (4), we found (1) α_{dust} = 0.91 ± 0.09 $m^2\ g^{-1}$ and (2) α_{dust} = 1.4 ± 0 1 $m^2\ g^{-1}$. This last value is higher as the soil mass estimated with equation (4) was lower than with the two other

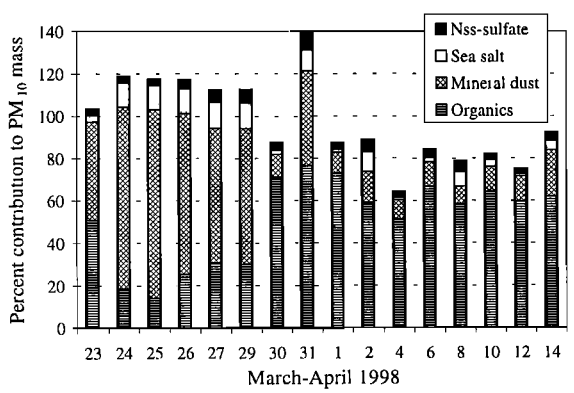

Figure 13. Percent contribution of aerosol types to the PM_{10} aerosol mass measured at Balbina for the period 23 March–14 April 1998. Apportionment is based on Chemical mass balance (CMB) calculations Nss-sulfate denotes non-sea-salt sulfate.

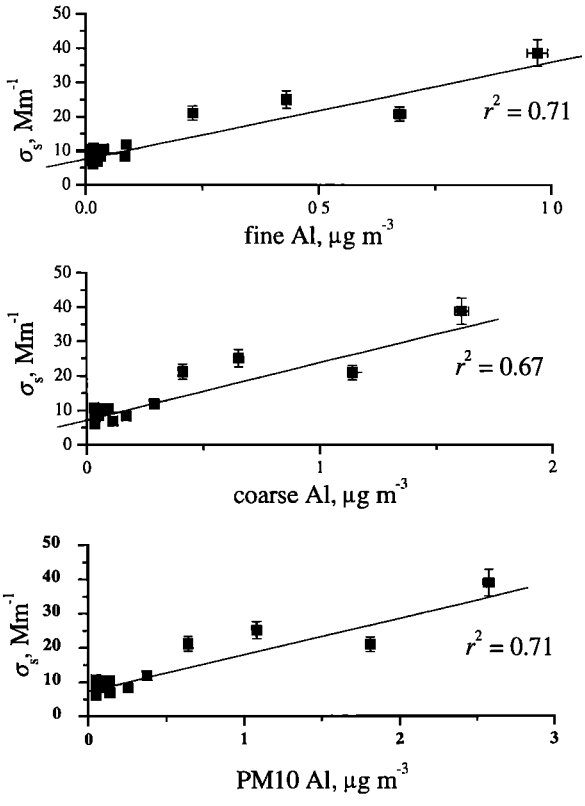

Figure 14. Linear regression of dry aerosol σ_s with respect to coarse, fine, and PM_{10} (sum of fine and coarse) Al concentrations during the dust event at Balbina. Error bars represent the experimental uncertainties.

models. In comparison, estimates of α_{dust} for the westward Saharan dust plumes have been reported by *Li et al.* [1996] at Barbados Island (α_{dust} between 0.77 (± 0.04) and 0.83 (± 0.04) m^2 g^{-1}) and by *Maring et al* [2000] (α_{dust} = 0 50 ± 0.10 m^2 g^{-1}) at Izaña.

In Israel, α_{dust} for the eastward Saharan plume was estimated by assuming the dust mass as the sum of aluminum silicate (calculated from measured Al) and $CaCO_3$ aerosols (from measured Ca). $CaCO_3$ is a major component of the soil dust in the Israeli desert [*Ganor and Mamane*, 1982; *Luria et al.*, 1996; *Formenti et al*, 2001]. During March 1998 the aerosol composition during the Saharan dust episodes showed clearly the signature of Ca (Table 2). The $CaCO_3$ fraction of the coarse soil mass averaged 50% (range 29–67%). Values of σ_s correlated with Al and Ca only in the coarse fraction, not in the fine. The resulting α_{dust} is 0.51 ± 0.05 m^2 g^{-1} (standard deviation equal to the fitting uncertainty, $r^2 = 0.92$).

Differences between the values of α_{dust} (Balbina, Sde Boker, and literature estimates) are not considered of physical significance and are rather attributed to the different dust matrix used and to the use of uncorrected scattering coefficients (Balbina and Sde Boker) Incidentally, we note that applying the angular truncation correction factor would further increase the discrepancy.

7. Conclusions

Saharan dust was detected in the lower troposphere over Suriname and Brazil during March 1998, when ground-based and airborne measurements were performed in the framework of the LBA-CLAIRE-98 experiment. Mineral dust transported from northern Africa dominated the aerosol load over the region. Occasional aged biomass burning plumes above 500 hPa, as well as anthropogenic pollution at the surface, were observed in Suriname. The Saharan dust layer generally extended up to 700 hPa over Suriname, and it exhibited a vertically uniform or a plume-like structure. Accumulation mode particles below 1 μm diameter accounted for up to 50% of the total column extinction.

In Brazil, Saharan mineral dust accounted for up to 70% of the PM_{10} mass, the lower limit being 50%. The ambiguity in the quantification of the mass associated with mineral dust depends upon the soil matrix model chosen for the calculation. Because of the dominance of dust on the aerosol mass, we were able to calculate the dry PM_{10} dust mass scattering efficiency (α_{dust}) using liner regression between the measured scattering coefficient and the mass of mineral dust. For various dust mass calculations, α_{dust} for the PM_{10} dust aerosols varied between 0.67 (± 0.07) and 1.4 (± 0.1) m^2 g^{-1}. In Israel, where the Saharan dust plume is enriched in Ca due to the high content of calcium carbonate of the local soil, α_{dust} was 0.51 ± 0.05 m^2 g^{-1} in the coarse fraction (compared to 1–1.5 m^2 g^{-1} in Brazil). An estimate of the PM_{10} α_{dust} was not done at Sde Boker because scattering did not correlate with fine dust.

Comparison of measurements in Tenerife and Suriname suggest that dry deposition is the major removal mechanism of coarse particles in the dust layers crossing the Atlantic Ocean, while wet removal is required additionally to explain removal of particles in the fine fraction. The implication of this is that coarse dust particles are rather hydrophobic, and as long as they do not mix with more hygroscopic components (sulfate from marine and/or pollution aerosols), they should not undergo major processing through the ITCZ. This is confirmed by the fact that the mass proportions of Al, Si, Ca, and Fe (major soil constituents) remain almost unvaried in Suriname and Brazil. The computational uncertainties on the column volume distributions and the correct apportionment of mineral dust to the aerosol fine fraction are the limiting factors to this discussion. Determining the extent to which the particle number concentration of these plumes is reduced would require additional sampling.

Organic aerosols emitted from the rain forest represented a secondary but important contribution to the aerosol load. We estimate organic aerosols to account for 50 to 90% of the PM_{10} mass at times when there is no Saharan mineral dust. Biogenic emissions account almost totally for the concentrations of P and OC, for which the contribution from mineral dust is of the order of 5%. The latter percentage is based on previous estimates of the organic fraction in mineral dust [*Li et al.*, 1996; *Prospero*, 1999]. The time limitation of the data set does not allow us to estimate optical parameters for organic aerosols, whose scattering mass efficiency is known only with large uncertainty but is of the same order of magnitude as scattering by sulfate particles [*Hegg et al*, 1997; *Novakov et al.*, 1997].

Notation

D_p	particle geometric diameter
EAD	particle equivalent aerodynamic diameter
$dV/d\log(D_p)$, $dV/d\log(\text{EAD})$	particle column volume distribution
σ_s	aerosol scattering coefficient
σ_a	aerosol absorption coefficient

τ_s	aerosol scattering optical depth
τ_a	aerosol extinction optical depth
α_{dust}	dust mass scattering efficiency
α_{Al}	aluminum mass scattering efficiency
FPM	fine particle mass (< 2 μm equivalent aerodynamic diameter)
CPM	coarse particle mass (2–10 μm equivalent aerodynamic diameter)
PM_{10}	sum of FPM and CPM (< 10 μm equivalent aerodynamic diameter)
TSP	total suspended particulate
OC	organic carbon
EC	elemental carbon
BC, BCE	black carbon, black carbon equivalent

Acknowledgments. This research was conducted as part of the Large-Scale Biosphere-Atmosphere Experiment in Amazonia (LBA), and is a contribution to the International Global Atmospheric Chemistry (IGAC) core project of the International Geosphere-Biosphere Program (IGBP). The financial support of the Max Planck Society, Munich, Germany, is gratefully acknowledged Three of us (J C., I R. and W.M) are indebted to the Belgian OSTC and the FWO-Vlaanderen for research support. P.A. acknowledges financial support from FAPESP. The technical and logistical support of the Citation air and ground crew is greatly appreciated. H. Maring (University of Miami) is acknowledged for providing the scattering data at Izaña, Tenerife, and for commenting on the manuscript. B. Stunder (NOAA Air Resources Laboratory, Maryland) provided us with the FNL meteorological database J. Herman (Laboratory for Atmospheres, Goddard Space Flight Center, Greenbelt, Maryland) provided the TOMS images shown in Figure 2. L. Orlovsky and A Karnieli (Remote Sensing Laboratory, Ben Gurion University of the Negev, Sde Boker, Israel) are thanked for sample collection and assistance in the nephelometer measurements at the Sde Boker site

References

Anderson, T. L , and J. A. Ogren, Determining aerosol radiative properties using the TSI 3563 integrating nephelometer, *Aerosol Sci Technol* , *29*, 57–69, 1998.

Andreae, M O., Soot carbon and excess fine potassium. Long-range transport of combustion derived aerosols, *Science*, *220*, 1148–1151, 1983.

Andreae, M O., Climatic effects of changing atmospheric aerosol levels, in *World Survey of Climatology*, vol. 16, *Future Climates of the World*, edited by A. Henderson-Sellers, pp. 341–392, Elsevier Sci., New York, 1995.

Andreae, M. O., Raising dust in the greenhouse, *Nature, 380*, 389–390, 1996.

Andreae, M. O , T. W Andreae, R. J. Ferek, and H. Raemdonck, Long-range transport of soot carbon in the marine atmosphere, *Sci. Total Environ* , *36*, 73–80, 1984.

Andreae, M. O., et al., Biomass-burning emissions and associated haze layers over Amazonia, *J Geophys Res* , *93*, 1509–1527, 1988.

Andreae, M. O., H. Berresheim, H. Bingemer, D. Jacob, S. M. Li, B. L. Lewis, and R. W. Talbot, The atmospheric sulfur cycle over the Amazon basin, 2, Wet season, *J Geophys. Res.*, *95*, 16,813–16,824, 1990

Andreae, M O , T W Andreae, H. J. Annegarn, J Beer, H. Cachier, P. le Canut, W Elbert, W. Maenhaut, I Salma, F. G Wienhold, and T. Zenker, Airborne studies of aerosol emissions from savanna fires in southern Africa, 2, Aerosol chemical composition, *J. Geophys. Res* , *103*, 32,119–32,128, 1998.

Andreae, M. O., et al., Transport of biomass burning smoke to the upper troposphere by deep convection in the equatorial region, *Geophys Res Letters*, *28*,951–954, 2001.

Artaxo, P., and H.-C. Hansson, Size distribution of biogenic aerosol particles from the Amazon basin, *Atmos Environ* , *29*, 393–402, 1995.

Artaxo, P., H. Storms, F. Bruynseels, R. Van Grieken, and W. Maenhaut, Composition and sources of aerosols from the Amazon basin, *J. Geophys. Res.*, *93*, 1605–1615, 1988.

Artaxo, P., W. Maenhaut, H. Storms, and R. Van Grieken, Aerosol characteristics and sources for the Amazon Basin during the wet season, *J. Geophys. Res* , *95*, 16,971–16,985, 1990.

Bergametti, G., L Gomes, G. Coude-Gaussen, P. Rognon, and M.-N. Le Coustumer, African dust observed over Canary Islands: Source-regions identification and transport pattern for some summer situations, *J. Geophys. Res* , *94*, 14,855–14,864, 1989.

Birch, M. E., and R. A. Cary, Elemental carbon-based method for monitoring occupational exposures to particulate diesel exhaust, *Aerosol Sci Technol* , *25*, 221-241, 1996

Chiapello, I , G Bergametti, B. Chatenet, P. Bousquet, F. Dulac, and E Santos Soares, Origins of African dust transported over the northeastern tropical Atlantic, *J Geophys Res* , *102*, 13,701–13,709, 1997

Chow, J. C., Measurement methods to determine compliance with ambient air quality standards for suspended particles, *J Air Waste Manage Assoc* , *45*, 320–382, 1995

Draxler, R. R., and G D. Hess, Description of the Hysplit_4 modeling system, *NOAA Tech Memo ERL, ARL-224*, 24 pp , 1997

Dubovik, O., A. Smirnov, B N Holben, M D King, Y. J. Kaufman, T. F. Eck, and I. Slutsker, Accuracy assessments of aerosol optical properties retrieved from AERONET Sun and sky-radiance measurements, *J Geophys. Res* , *105*, 9791-9806, 2000.

Echalar, F., P. Artaxo, J. Vanderlei Martins, M. Yamasoe, F. Gerab, W. Maenhaut, and B. Holben, Long-term monitoring of atmospheric aerosols in the Amazon basin: Source identification and apportionment, *J. Geophys Res.*, *103*, 31,849–31,864, 1998.

Foner, H. A., and E Ganor, The chemical and mineralogical composition of some urban atmospheric aerosols in Israel, *Atmos. Environ* , *26*, 125–133, 1992.

Formenti, P., M. O. Andreae, and J Lelieveld, Measurements of aerosol optical depth above 3570 m asl in the North Atlantic free troposphere: Results from ACE-2, *Tellus*, *52B*, 678–693, 2000.

Formenti, P., M. O. Andreae, T. W. Andreae, C Ichoku, G. Schebeske, A. J. Kettle, W. Maenhaut, J. Cafmeyer, J Ptasinsky, A. Karnieli, and J Lelieveld, Physical and chemical characteristics of aerosols over the Negev Desert (Israel) during summer 1996, *J Geophys Res* , *106*, 4871–4890, 2001

Ganor, E , The frequency of Saharan dust episodes over Tel Aviv, Israel, *Atmos Environ* , *28*, 2867–2871, 1994

Ganor, E , and Y. Mamane, Transport of Saharan dust across the eastern Mediterranean, *Atmos Environ.*, *16*, 581–587, 1982.

Gassó, S., D A. Hegg, D. S. Covert, D. Collins, K Noone, E. Öström, B. Schmid, P. B. Russell, J. M. Livingston, P. A Durkee, and H. Jonsson, Influence of humidity on the aerosol scattering coefficient and its effect on the upwelling radiance during ACE-2, *Tellus*, *52B*, 546–565, 2000.

Gaudichet, A., F. Echalar, B. Chatenet, J. P Quisefit, G. Maligret, H Cachier, P Buat-Menard, P Artaxo, and W. Maenhaut, Trace elements in tropical African savanna biomass burning aerosols, *J Atmos Chem* , *22*, 19–39, 1995.

Gordon, G. E., Receptor models, *Environ Sci. Technol* , *22*, 1132–1142, 1988.

Gregory, G. L., et al., Air chemistry over the tropical forest of Guyana, *J. Geophys Res* , *91*, 8603–8612, 1986.

Hegg, D. A., J. Livingston, P. V. Hobbs, T. Novakov, and P. Russell, Chemical apportionment of aerosol column optical depth off the mid-Atlantic coast of the United States, *J. Geophys Res* , *102*, 25,293–25,303, 1997.

Herman, J P., P K. Barthia, O. Torres, C. Hsu, C Seftor, and E. Celarier, Global distribution of UV-absorbing aerosols from NIMBUS 7/TOMS data, *J Geophys Res.*, *102*, 16,911–16,922, 1997.

Holben, B. N., et al., AERONET—A federated instrument network and data archive for aerosol characterization, *Rem. Sens Environ.*, *66*, 1–16, 1998.

Husar, R. B., J. M. Prospero, and L. L. Stowe, Characterization of tropospheric aerosols over the oceans with the NOAA advanced very high resolution radiometer optical thickness operational product, *J. Geophys Res* , *102*, 16,889–16,909, 1997.

Jaenicke, R , Tropospheric aerosols, in *Aerosol-Cloud-Climate*

Interactions, edited by P. V. Hobbs, pp. 1–31, Academic, San Diego, Calif., 1993.

Jaenicke, R., Atmospheric aerosol size distribution, in *Atmospheric Particles*, edited by R. M. Harrison and R. E. van Grieken, pp. 1–28, John Wiley, New York, 1998.

King, M. D., D. M. Byrne, B. M. Herman, and J. A. Reagan, Aerosol size distributions obtained by inversion of spectral optical depth measurements, *J. Atmos. Sci*, *35*, 2153–2167, 1978.

Li, X., H. Maring, D. Savoie, K. Voss, and J. M. Prospero, Dominance of mineral dust in aerosol light-scattering in the North Atlantic trade winds, *Nature*, *380*, 416–419, 1996.

Li-Jones, X., and J. M. Prospero, Variations in the size distribution of non-sea-salt sulfate aerosol in the marine boundary layer at Barbados: Impact of African dust, *J. Geophys. Res.*, *103*, 16,073–16,084, 1998.

Li-Jones, X., H. B. Maring, and J. M. Prospero, Effect of relative humidity on light scattering by mineral dust as measured in the marine boundary layer over the tropical Atlantic Ocean, *J. Geophys. Res.*, *103*, 31,113–31,121, 1998.

Luria, M., M. Peleg, G. Sharf, D. S. Tov-Alper, N. Spitz, Y. Ben Ami, Z. Gawii, B. Lifschitz, A. Yitzchaki, and I. Seter, Atmospheric sulfur over the east Mediterranean region, *J. Geophys. Res.*, *101*, 25,917–25,930, 1996.

Maenhaut, W., and H. Raemdonck, Accurate calibration of a Si(Li) detector for PIXE analysis, *Nucl. Instrum Methods Phys. Res.*, Sect. *B* 1, 123–136, 1984.

Maenhaut, W., and W. H. Zoller, Determination of the chemical composition of the South Pole aerosol by instrumental neutron activation, *J Radioanal. Chem.*, *37*, 637–650, 1977.

Maenhaut, W., R. Hillamo, T. Mäkelä, J. L. Jaffrezo, M. H. Bergin, and C.I. Davidson, A new cascade impactor for aerosol sampling with subsequent PIXE analysis, *Nucl. Instrum. Methods Phys. Res. Sect. B 109/110*, 482–487, 1996a.

Maenhaut, W., G. Koppen, and P. Artaxo, Long term atmospheric aerosol study in Cuiabá, Brazil: Multielemental composition, sources, and impacts of biomass burning, in *Biomass Burning and Global Change*, edited by Joel Levine, pp. 637–652, MIT Press, Cambridge, Mass., 1996b.

Maring, H., D. L. Savoie, M. A. Izaguirre, C. McCormick, R. Arimoto, J. M. Prospero, and C. Pilinis, Aerosol physical and optical properties and their relationship to aerosol composition in the free troposphere at Izaña, Tenerife, Canary Islands, during July 1995, *J Geophys. Res*, *105*, 14,677–14,700, 2000.

Mason, B., *Principles of Geochemistry*, 3rd ed., John Wiley, New York, 1966.

Moulin, C., F. Dulac, C. E. Lambert, P. Chazette, I. Jankowiak, B. Chatenet, and F. Lavenu, Long-term daily monitoring of Saharan dust load over ocean using Meteosat ISCCP-B2 data, 2, Accuracy of the method and validation using sunphotometer measurements, *J. Geophys. Res.*, *102*, 16,959–16,969, 1997.

Moulin, C., et al., Satellite climatology of African dust transport in the Mediterranean atmosphere, *J. Geophys. Res.*, *103*, 13,137–13,144, 1998.

Nemeruyk, G. E., Migration of salts into the atmosphere during transpiration, *Sov. Plant Physiol.*, *17*, 560–566, 1970.

Novakov, T., C. E. Corrigan, J. E. Penner, C. C. Chuang, O. Rosario, and O. L. Mayol Bracero, Organic aerosols in the Carribean trade winds: A natural source?, *J. Geophys. Res.*, *102*, 21,307–21,314, 1997.

Patterson, E. M., D. A. Gillette, and B. H. Stockton, Complex index of refraction between 300 and 700 nm for Saharan aerosols, *J. Geophys. Res*, *82*, 3153–3160, 1977.

Perry, K. D., T. A. Cahill, R. A. Eldred, D. D. Dutcher, and T. E. Gill, Long-range transport of North African dust to the eastern United States, *J. Geophys. Res.*, *102*, 11,225–11,238, 1997.

Prospero, J. M., Long-term measurements of the transport of African mineral dust to the southeastern United States: Implications for regional air quality, *J. Geophys. Res.*, *104*, 15,917–15,927, 1999.

Prospero, J. M., and T. N. Carlson, Vertical and areal distribution of Saharan dust over the western equatorial North Atlantic Ocean, *J. Geophys. Res.*, *77*, 5255–5265, 1972.

Prospero, J. M., R. A. Glaccum, and R. T. Nees, Atmospheric transport of soil dust from Africa to South America, *Nature*, *289*, 570–572, 1981.

Reid, J. S., and P. V. Hobbs, Physical and optical properties of young smoke from individual biomass fires in Brazil, *J. Geophys. Res.*, *103*, 32,013–32,030, 1998.

Reid, J. S., P. V. Hobbs, R. J. Ferek, D. R. Blake, J. Vanderlei Martins, M. R. Dunlap, and C. Liousse, Physical, chemical and optical properties of regional hazes dominated by smoke in Brazil, *J. Geophys. Res.*, *103*, 32,059–32,080, 1998.

Riley, J. P., and R. Chester, *Introduction to Marine Chemistry*, Academic, San Diego, Calif., 1971.

Scheele, M. P., P. C. Siegmund, and P. F. J. Van Velthoven, Sensitivity of trajectories to data resolution and its dependence on the starting point: In or outside a tropopause fold, *Meteorol. Appl.*, *3*, 267–273, 1996.

Schmid, B., et al., Clear sky closure studies of lower tropospheric aerosol and water vapor during ACE-2 using airborne sunphotometer, airborne in-situ, space-borne, and ground-based measurements, *Tellus*, *52B*, 568–593, 2000.

Seinfeld, J. H., and S. N. Pandis, *Atmospheric Chemistry and Physics: From Air Pollution to Climate Change*, 1360 pp., John Wiley, New York, 1997.

Swap, R., M. Garstang, S. Greco, R. Talbot, and P. Kållberg, Saharan dust in the Amazon basin, *Tellus*, *44B*, 133–149, 1992.

Talbot, R. W., R. C. Harriss, E. V. Browell, G. L. Gregory, D. I. Sebacher, and S. M. Beck, Distribution and geochemistry of aerosols in the tropical North Atlantic troposphere: Relationship to Saharan dust, *J. Geophys Res.*, *91*, 5173–5182, 1986.

Taylor, S. R., and S. M. McLennan, *The Continental Crust. Its Composition and Evolution*, Blackwell, Malden, Mass., 1985.

Tegen, I., and A. A. Lacis, Modeling of particle size distribution and its influence on the radiative properties of mineral dust aerosol, *J. Geophys. Res.*, *101*, 19,237–19,244, 1996.

Turpin, B. J., P. Saxena, and E. Andrews, Measuring and simulating particulate organics in the atmosphere: Problems and prospects, *Atmos Environ.*, *34*, 2983–3013, 2000.

M. O. Andreae, P. Formenti, L. Lange, and G. Roberts, Biogeochemistry Department, Max Planck Institute for Chemistry, P. O. Box 3060, D-55020 Mainz, Germany. (pfo@mpch-mainz.mpg.de)

P. Artaxo, Instituto de Física, Universidade de São Paulo, Caixa Postal 66318, CEP 05389-970, São Paulo, Brazil.

J. Cafmeyer, W. Maenhaut, and I. Rajta, Institute for Nuclear Sciences, University of Gent, Proeftuinstraat 86, B-9000 Gent, Belgium.

B. N. Holben, NASA Goddard Space Flight Center, Biospheric Sciences Branch, Greenbelt, MD 20771.

J. Lelieveld, Institute for Marine and Atmospheric Research (IMAU), Princetonplein 5, University of Utrecht, 3584 CC Utrecht, Netherlands.

(Received May 17, 2000; revised October 30, 2000;
accepted November 14, 2000.)